Neuroscience Research 74 (2012) 17–24

Contents lists available at SciVerse ScienceDirect

Neuroscience Research

journal homepage: www.elsevier.com/locate/neures

Quantitative analysis of zinc in rat hippocampal mossy fibers by nuclear microscopy

Binbin Zhang[a,b], Minqin Ren[c], Fwu-Shan Sheu[a,d,*], Frank Watt[c,**], Aryeh Routtenberg[e,***]

[a] Nanoscience & Nanotechnology Initiative, National University of Singapore, 2 Engineering Drive 3, Singapore 117581, Singapore
[b] Department of Biological Sciences, National University of Singapore, 14 Science Drive 4, Singapore 117543, Singapore
[c] Centre for Ion Beam Applications, Department of Physics, National University of Singapore, 2 Science Drive 3, Singapore 117542, Singapore
[d] Department of Electrical and Computer Engineering, National University of Singapore, Singapore
[e] Department of Psychology, Neurobiology and Physiology, and the Northwestern University Institute for Neuroscience (NUIN), Northwestern University, 2029 Sheridan Road, Evanston, IL 60208, USA

ARTICLE INFO

Article history:
Received 17 May 2012
Received in revised form 21 June 2012
Accepted 22 June 2012
Available online 2 July 2012

Keywords:
Quantitative analysis
Zn concentration
Hippocampal mossy fibers
Nuclear microscopy
PIXE
STIM
RBS

ABSTRACT

Zinc (Zn) is involved in regulating mental and motor functions of the brain. Previous approaches have determined Zn content in the brain using semi-quantitative histological methods. We present here an alternative approach to map and quantify Zn levels in the synapses from mossy fibers to CA3 region of the hippocampus. Based on the use of nuclear microscopy, which is a combination of imaging and analysis techniques encompassing scanning transmission ion microscopy (STIM), Rutherford backscattering spectrometry (RBS), and particle induced X-ray emission (PIXE), it enables quantitative elemental mapping down to the parts per million (μg/g dry weight) levels of zinc in rat hippocampal mossy fibers. Our results indicate a laminar-specific Zn concentration of 240 ± 9 μM in wet weight level (135 ± 5 μg/g dry weight) in the stratum lucidum (SL) compared to 144 ± 6 μM in wet weight level (81 ± 3 μg/g dry weight) in the *stratum pyramidale* (SP) and 78 ± 10 μM in wet weight level (44 ± 5 μg/g dry weight) in the *stratum oriens* (SO) of the hippocampus. The mossy fibers terminals in CA3 are mainly located in the SL. Hence the Zn concentration is suggested to be within this axonal presynaptic terminal system.

1. Introduction

Zn is an essential element for sustaining life. It is the second most abundant trace metal after iron (Fe) in the mammalian tissues (Vallee and Falchuk, 1993; Lippard and Berg, 1994). It has been reported that Zn constitutes as essential structural component of DNA, RNA and ribosome (MacDonald, 2000). In addition to acting as a cofactor, it stabilizes several hundreds of enzymes and other proteins (Vallee and Falchuk, 1993; Tupler et al., 2001). In the human genome, Zn-binding proteins participate in transcription regulation (Tupler et al., 2001). Zn thus regulates numerous processes involved in cellular metabolism, gene expression, nucleic acid repair, cell replication, tissue repair and growth, and development (Fujii, 1954; Fujii et al., 1955; Prasad et al., 1961; Vallee and Auld, 1993a,b; O'Halloran, 1993; Prasad, 1996; Berg and Shi, 1996; Coleman, 1998; Wood, 2000; Daiyasu et al., 2001; Truong-Tran et al., 2001; Ho and Ames, 2002; Brown et al., 2002).

The mammalian central nervous system (CNS) contains an abundance of Zn. There are three main sources of Zn (total zinc) in the brain, which are (1) vesicular pool in the synaptic vesicle; (2) membrane-bound, metalloprotein, or protein-metal complex pool; and (3) ionic pool of free or loosely bound ions in the cytoplasm (Frederickson, 1989). Among these, the metallocomplex pools of Zn, which are involved in both metabolic reactions and structural support for biomembranes and protein folds, could not be detected by histochemical staining method (i.e. Timm's stain) due to its strong complexation with proteins and location of Zn deep within the protein structures. In addition, there exist very low concentrations of an intracellular ionic Zn because of a number of zinc-binding proteins in brain tissues. Therefore, the vesicular Zn pool is quantitatively the most significant through histochemical detection.

Histochemical studies have revealed that accumulations of reactive or free zinc (Zn^{2+}) in the brain are mostly sequestered

* Corresponding author at: Nanoscience & Nanotechnology Initiative, Blk E3-05-29, National University of Singapore, 2 Engineering Drive 3, Singapore 117581, Singapore. Tel.: +65 6516 2857; fax: +65 6872 5563.
** Corresponding author at: Department of Physics, Blk S12, National University of Singapore, 2 Science Drive 3, Singapore 117542, Singapore. Tel.: +65 6516 2815; fax: +65 6777 6126.
*** Corresponding author at: Department of Psychology, Neurobiology and Physiology, and the Northwestern University Institute for Neuroscience (NUIN), Swift Hall Room 102, Northwestern University, 2029 Sheridan Road, Evanston, Illinois 60208, USA. Tel.: +1 847 491 3628; fax: +1 847 491 3557.
E-mail addresses: elesfs@nus.edu.sg (F.-S. Sheu), phywattf@nus.edu.sg (F. Watt), aryeh@northwestern.edu (A. Routtenberg).

0168-0102/$ – see front matter © 2012 Elsevier Ireland Ltd and the Japan Neuroscience Society. All rights reserved.
http://dx.doi.org/10.1016/j.neures.2012.06.004

within the vesicles of glutamatergic synapses (Frederickson, 1989; Frederickson and Moncrieff, 1994; Frederickson et al., 2000; Paoletti et al., 2009). These Zn^{2+}-containing vesicles are particularly numerous in mossy fiber (MF) synapses in the CA3 region in hippocampus and a variety of forebrain areas. It has been shown that Zn^{2+} is co-released with glutamate from MFs terminals in the same manner as neurotransmitters, and is necessary for the induction of long-term potentiation (LTP) at hippocampal mossy fibers to CA3 pathway (Li et al., 2001; Huang et al., 2008). Furthermore, Zn^{2+} is known to interact with the protein kinases thereby triggering intracellular signal transduction pathways that affect changes in the gene expression (Brewer et al., 1979; Hubbard et al., 1991; Weinberger and Rostas, 1991; Quest et al., 1992; Maret et al., 1999; Park and Koh, 1999; Lengyel et al., 2000; Besser et al., 2009).

Due to the critical biological functions of Zn^{2+} in the brain, the regulation of Zn^{2+} concentration is very important for brain health and its performance. Indeed, the redistribution of Zn^{2+}-containing MFs has been strongly linked to the formation of long-lasting memory (Routtenberg, 2010). Localization of Zn^{2+} and observation of cellular Zn^{2+} levels become necessary for investigations on the Zn associated neurological dysfunctions and diseases. In previous studies, Zn was detected using techniques such as histochemical staining (Timm's staining) methods, fluorescence labeling methods (Frederickson et al., 1989) and stable-isotope dilution. The Timm's sulfide/silver staining technique detects free Zn (Zn^{2+}) in mammalian brain, which is highly concentrated in the hippocampal mossy fibers terminals (Danscher, 1981, 1996; Danscher et al., 1985). Histochemical studies are ideal for assessing chemical spatial profiles, but in general are not quantitative. Studies using stable-isotope dilution mass spectrometry Frederickson et al., 1983) have shown that the hippocampal Zn concentrations were in a range of 77.2 to 92.7 ppm, and the amount of Zn directly associated with MFs vesicles was estimated to be approximately 8% of the total zinc in the hippocampus. The Zn concentration in the vesicles of the MFs can therefore be estimated at 220–300 μM. Although stable-isotope dilution mass spectrometry is currently considered the most accurate and precise method for quantitative elemental concentrations, it is essentially a bulk analysis technique and accurate sampling of the required area is difficult. The use of nuclear microscopy, with its elemental and structural mapping capability, is able to image specific areas of tissue sections with high quantitative and spatial accuracy, but is unable to differentiate between the chemical states of the elements detected, i.e. the total amounts of Zn, including both free (Zn^{2+}) and co-factor bond form of Zn to proteins, are measured.

Nuclear microscopy is a technique relying on the interaction between a focused beam of MeV protons and the specimen. It is composed of three ion beam related techniques, i.e. particle induced X-ray emission (PIXE) for trace elemental analysis, Rutherford backscattering spectrometry (RBS) (Watt, 1995 and Watt et al., 2006) for matrix characterization and scanning transmission ion microscopy (STIM) for structural identification. PIXE is a technique where incoming MeV protons collide with inner shell electrons of the target atom, and any resulting electronic vacancies are filled by outer shell electrons. The re-arrangement of the atomic electronic structure results in the emission of a characteristic X-ray photon, the energy of which is unique to the parent atom. By measuring the energy of the X-ray photon the parent atom can be identified. STIM is a technique based on mapping of the energy loss of transmitted protons, which depends on the density of samples. It is used for the structural imaging and fast positioning of the samples without chemical fixing and staining. The trace elemental mapping was carried out by the nondestructive technique PIXE (Johansson et al., 1995), which can perform simultaneous detection of multiple elements with high quantitative accuracy and with a sensitivity of down to 1 μg/g dry weight. PIXE is similar in principle to electron induced X-ray emission (e.g. EDX), except that in EDX the bremsstrahlung background radiation prevalent when primary electrons are used limits the elemental sensitivity to around 1 part in 10^4, thus precluding the use of this technique for trace elemental studies. RBS is a technique where the incoming protons are backscattered from atomic nuclei, and is efficient in the measurement of light elements such as those found in the organic tissue matrix i.e. carbon, nitrogen, and oxygen. Therefore, RBS is used to provide information on the thickness and matrix composition, area density of the sample, as well as calculating the charge collected during each measurement.

The strength of nuclear microscopy lies in its capability of elemental mapping at μg/g dry weight level, which is equivalent to measuring Zn concentrations down to 1.8 μM in wet tissues in the current study, and the ability to measure the concentrations of trace elements with high quantitative accuracy independent of the chemical state of the element. Therefore, nuclear microscopy is ideally suited for imaging the morphology of tissues and mapping the trace elements such as Fe, Ca, Zn and Cu (Ren et al., 2003, 2006; Rajendran et al., 2009; Watt et al., 2006).

Previous studies have been performed for trace elemental analysis of Zn in rat hippocampus using nuclear microscopy through the technique of proton induced X-ray emission (PIXE). It has been shown that the mean concentration of Zn was detected at 120 ppm (dry weight) in non-fixed hippocampus (Kemp and Danscher, 1979). Furthermore, the maximum MFs Zn level was calculated using PIXE by Wensink and his colleagues in 1987. With the proton micro beam focused to 60 μm × 60 μm, 2 mm line scans were made across the hippocampal hilar region to extract the value of 136 ppm (dry weight) of Zn level in the MFs located in the hilar area. However, evidences on absolute Zn concentrations in the laminar structure of MF terminals are still vacant. Because of the critical function of Zn as neurotransmitters in the MFs terminals, it is essential to quantify Zn in synapses of the MFs to CA3 neurons. Hippocampal CA3 is composed of three layers, which are defined as *stratum lucidum* (SL), *stratum pyramidale* (SP) and *stratum oriens* (SO) respectively. SO is the second superficial layer, where the basal dendrites of CA3 pyramidal neurons locate. SP is the pyramidal neurons layer, containing synapses from the mossy fibers which course through SL. SL is the inner layer next to SP in CA3, where mossy fibers from granule cells of the dentate gyrus course through and terminate with synapses to the CA3 pyramidal neurons in SP. It has been demonstrated that most of the Zn^{2+} is sequestered within the vesicles of mossy fiber glutamatergic synapses (Frederickson, 1989; Frederickson and Moncrieff, 1994; Frederickson et al., 2000). Therefore, there may be laminar difference of Zn concentrations between the three layers in CA3. However, no studies on laminar-specific concentration of Zn in CA3 have been reported so far.

In this study, nuclear microscopy based imaging techniques were employed in order to accurately identify and quantify Zn in the brain, especially in the synapses from mossy fibers to CA3 in the hippocampus. In addition, high resolution nuclear microscopy that focuses to a 1 μm spot size was applied to provide structural and elemental images of the hippocampus, in order to measure the concentrations of total Zn in the SL, the layer containing the most synapses of hippocampal mossy fibers in CA3 region, and the two adjacent layers: the SP and SO.

2. Materials and methods

2.1. Animals and tissue preparations

Seven adult male Sprague-Dawley rats, aged 6–7 weeks, were used. All protocols including animal handling and tissue collections

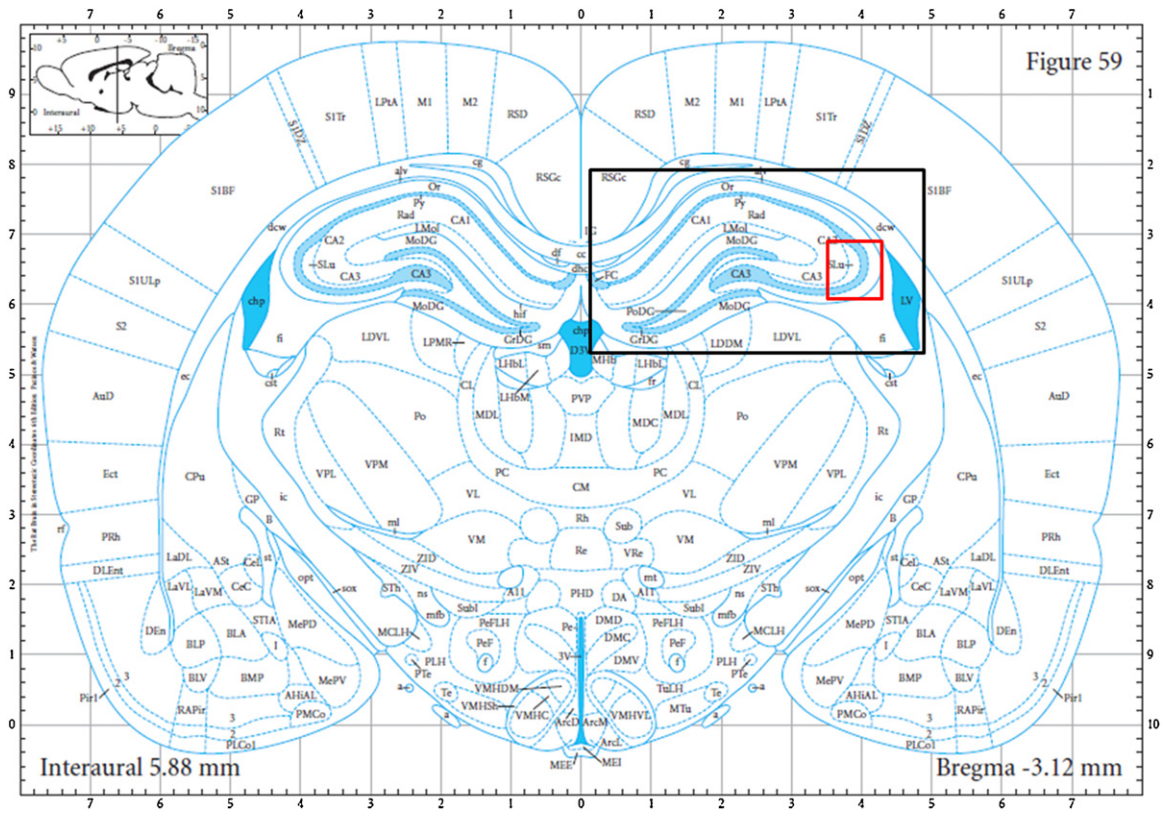

Fig. 1. Brain atlas at −3.12 mm from bregma considered as the position reference (This map is taken and referred from Paxinos and Watson, 6th edition with permission). Black rectangle area containing the hippocampus was scanned for PIXE analysis and red rectangle area was selected for further elemental analysis. (For interpretation of the references to color in this figure legend, the reader is referred to the web version of the article.)

were approved by the Institutional Animal Care and Use Committee (IACUC) of National University of Singapore.

Animals were sacrificed by intraperitoneal injection of a mixture composed of ketamine (70 mg/kg) and xylazine (8 mg/kg). Brains were quickly extracted, and blocks containing the hippocampus were removed. Blocks were covered with the embedding material Jung Tissue-Freezing Medium (Leica Instruments, Germany) and frozen immediately with liquid nitrogen within minutes of removal. The samples were transported on dry ice whenever required and stored at −80 °C. 20 μm thick slices of the dorsal hippocampus were sectioned coronally using a cryostat (Jung Frigocut 2800E, Leica, Nussloch, Germany) at −16 °C. The positions of the coronal sections were around −3 to −3.2 mm from bregma with the reference brain atlas shown in Fig. 1 (Paxinos and Watson, 2007). These sections were picked up on freshly prepared submicron pioloform films, which were mounted on the nuclear microscope target holders and freeze–dried at −20 °C. Adjacent sections were then mounted on the polylysine-coated glass slides (Polyscience, Inc., USA.) for Timm's staining.

2.2. Histology analysis

2.2.1. Timm's staining

Firstly, the tissues were submerged initially in 1% sodium sulfide (Na_2S) for 10 min and then in 3% glutaraldehyde/4% paraformaldehyde/0.1 M PBS, pH 7.4 for 10 min. After that, they were developed in a Timm's stain solution composed of 50% (w/v) Arabic gum (120 mL), 5% (w/v) hydroquinone (60 mL), citric acid (20 mL) and silver nitrate (500 μL) at 30 °C for 90 min in absolutely dark. Then tissues were rinsed in deionized water (DIW) for 10 min and counterstained with cresyl violet.

2.2.2. Nissl staining

The sections were stained with 0.1% cresyl violet for 15 min and consequently rinsed three times with 90% (v/v) ethanol followed by rinsing three times with xylene to dehydrate. Finally, the sections were mounted and observed by optical microscopy.

2.3. Mapping and quantifying Zn: nuclear microscopy

The samples were scanned using the nuclear microscope at the Center for Ion Beam Applications (CIBA), Department of Physics, National University of Singapore (Watt, 1995). The nuclear microscopy was carried out using a 2-MeV proton beam focused to a 1 μm spot size (Watt et al., 1994). The complementary techniques of PIXE, RBS, and STIM were simultaneously used in the analysis. Nuclear microscopy measurements were carried out to observe the overall distribution of the elements in the hippocampus. To examine the spatial distribution of Zn in the areas of interest, different scan sizes ranging from 4 mm to 600 μm were measured. The spatial resolution was concerned during the measurement. When large area imaging (e.g. 2–4 mm) was carried out, the spatial resolution was about 3–4 μm in order to have more beam and when small region (e.g. 200–600 μm) measurement was carried out, the spatial resolution was about 1 μm. Each measurement was multiple scans over the same area of interest for about 45 min with a beam current of about 100 pA. The data from all these three techniques was recorded using the data acquisition system OMDAQ (Oxford Microbeams Data Acquisition System, Oxford Microbeams Ltd., Oxford) (Grime and Dawson, 1994). The trace elemental concentrations in μg/g dry weights level were extracted from the region of interest and analyzed.

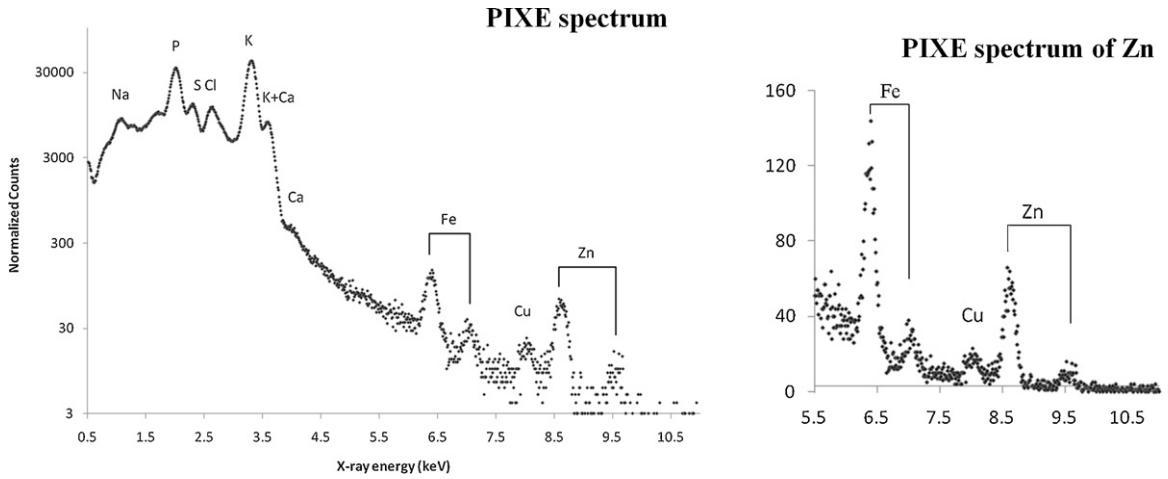

Fig. 2. PIXE energy spectrum of the hippocampus showing characteristic X-ray peaks: Plotted as a log plot. The figure on the RHS is a linear plot of the PIXE spectrum in the energy range 5.5–11 keV, showing the peaks corresponding to Fe, Cu and Zn.

3. Results

3.1. Elemental mapping of hippocampus

The hippocampus tissue sections were scanned using a 2 MeV proton beam. The proton induced emission of X-rays of different elements were measured simultaneously using an energy dispersive X-ray detector, which was fitted with a filter designed as 300 μm thickness perspex with a central hole of 1 mm in diameter for optimal detection of trace elements above calcium in the periodic table. For a multiple-element sample, the PIXE spectrum consists of a number of peaks which correspond to the characteristic emission X-rays from the elements in the sample. As shown in Fig. 2, multiple elemental peaks extracted from the large area scan can be observed. The peak at 8.6 keV corresponds to the Zn Kα X-ray line. Fig. 2 also shows the peaks corresponding to copper (Cu) and iron (Fe), trace metals not easily quantified using other techniques.

STIM was used to facilitate positioning of the samples to regions of interest. STIM provides information on mass density distribution of the sample by analyzing the transmitted proton energy using a silicon surface barrier detector placed behind the target sample in an off-axis position. STIM mapping enables the mass density of the whole hippocampus (Fig. 3B) to be imaged. Timm's stain images of the adjacent sections showed the Zn^{2+} distribution in hippocampus (Fig. 3A), thus providing reference points in the identification of substructures in the hippocampus. In the current study, detection of the distribution and concentration of Zn was focused on the hippocampal CA3 area. A reduced area scan of 2 mm was therefore carried out in the region of interest (ROI), and the corresponding STIM image is shown in Fig. 3C.

3.2. Zn profile by line scan in CA3

In order to verify the distribution of Zn throughout the projection zone of mossy fibers to CA3, a line scan was carried out. The structural STIM maps of the areas chosen for high-resolution studies are shown in Fig. 4A and B. Given that the decreasing concentration of Zn from SL to SP and SO in CA3, the line scan across the CA3 layers as depicted by the dotted black line in Fig. 4B was performed. The line scan plot of Zn profile, indicated by the number of Zn X-ray photons detected along the line scan versus marked line scan distance, showed the highest concentration in SL followed by SP and SO (Fig. 4C), and is consistent with the Timm's stained adjacent section (Fig. 3A). The line scans across the layers of CA3 provide an estimation of Zn present in the various structural layers.

3.3. Quantitative analysis of Zn

To further elucidate the distribution throughout the layers of CA3, higher resolution studies were carried out. On the basis of Zn profile in layers of CA3 extracted by line scan in Fig. 4, a reduced scan of 600 μm over a selective region of CA3 covering SL-SP-SO was chosen. The section analyzed was unstained and therefore free from contaminants. The structural STIM image and the PIXE zinc map of the area chosen for high-resolution studies are shown in Fig. 5A and B. Strata of SL and SP and SO were indentified based on the STIM density and the correlations with Timm's staining of adjacent sections. The higher-resolution studies showed that the highest accumulation of zinc was in SL among the 3 layers of CA3 (Fig. 5B). A broad line scan was then carried out crossing the strata from SL down to SO and the outer region, as depicted by the dotted red down arrow (Fig. 5B). The plot of X-ray counts of Zn versus marked line scan distance showed pronounced changes in the Zn level among the various layers of CA3 (Fig. 5C).

The concentration of Zn, as well as Fe and Cu, in each layer of CA3 was given based on the information extracted from the whole area as indicated in Fig. 5A. The averages were made among seven sections of seven rats, and the standard error of mean was given. Based on quantitative results from the nuclear microscopy measurements indicated in Table 1, a significant higher concentration of Zn was observed for the SL (135 ± 5 μg/g dry weight) compared with the SP (81 ± 3 μg/g dry weight; Student's *t*-test, $^{**}p < 0.0001$) and the SO (44 ± 5 μg/g dry weight; Student's *t*-test, $^{**}p < 0.0001$), which were in accordance with the maximum Zn value of 136 ppm in the MFs in the hilar (Wensink et al., 1987). In comparison to Zn, the average concentrations of Fe from SL and SP were extracted at similar lower levels of 53 ± 2.4 μg/g dry weight and 50 ± 2.0 μg/g dry weight respectively (Student's *t*-test, $p = 0.51$). In addition, it appeared much lower value in SO (36 ± 2.4 μg/g dry weight) com-

Table 1
Average concentrations and standard errors of Fe Cu and Zn in different layers and background levels, based on seven sections from seven rats.

Layer	Zn (μg/g)	Fe (μg/g)	Cu (μg/g)
SL	135 ± 5.3	53 ± 2.4	8.0 ± 2.1
SP	81 ± 3.3	50 ± 2.0	8.0 ± 1.7
SO	44 ± 5.4	36 ± 2.4	9.0 ± 2.0
Background	20 ± 1.5	16 ± 1.0	5.0 ± 0.9

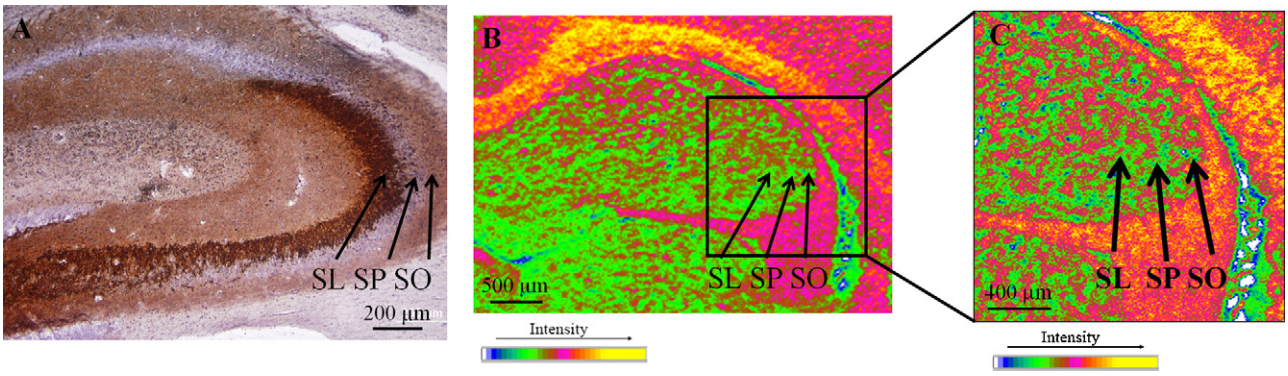

Fig. 3. Images of the region of interest CA3: (A) Timm's staining; (B) STIM image of the region of interest (C) STIM image (image size 2 mm × 2 mm). (SL: *stratum oriens*; SP: *stratum pyramidale*; SL: *stratum lucidum*). The intensity of color scale indicates changes of the area density from low to high. (For interpretation of the references to color in this figure legend, the reader is referred to the web version of the article.)

paring to SL (Student's *t*-test, $^{*}p < 0.05$) and SP (Student's *t*-test, $^{*}p < 0.05$). It has been reported that the highest concentrations of iron in the hippocampus were observed in dentate gyrus (Drayer et al., 1986; Schenck, 2003; Jackson et al., 2006). Therefore, it is in accordance that higher Fe concentration was detected in SL and SP than SO. As shown in the PIXE spectrum of the whole hippocampus, higher peaks corresponding to Fe than Zn were obtained (Fig. 2). In contrast, the Fe contents in CA3 were detected much lower than those of Zn, suggesting an uncorrelated distribution patterns between Fe and Zn in rat CA3 layers of the hippocampus. Regarding the levels of Cu, values in the three layers of CA3 were very close (8.0 ± 2.1 μg/g dry weight in SL; 8.0 ± 1.7 μg/g dry weight in SP; and 9.0 ± 2.0 μg/g dry weight in SO (Student's *t*-test, $p > 0.05$). Previous study has reported that Cu is distributed throughout most regions of the rat brain and is most abundant in the medial geniculate nucleus, part of the superior colliculus, and the periaqueductal grey (Jackson et al., 2006; Lutsenko et al., 2010). However, Cu levels in the hippocampus are moderate, indicating a uniform distribution of Cu in the MFs terminal to CA3. Since the original tissue sections were cut 20 μm thick, based on the mean matrix mass area density of the scanning areas, then the Zn concentration in dry weight converts to 240 ± 9 μM in the SL compared to 144 ± 6 μM in the SP and 78 ± 10 μM in the SO in wet tissues. This result is consistent with previous determinations of the Zn^{2+} concentration in the vesicles of the mossy fibers of between 220 μM and 300 μM (Frederickson et al., 1983). Since nuclear microscopy detects the total amounts of Zn in targeted area, including both free (Zn^{2+}) and co-factor bond form of Zn to proteins, the concentration of co-factor bond Zn in the area outside of the MFs was considered as the mean background Zn level. The mean background Zn level was calculated at 35.5 ± 2.7 μM (20 ± 1.5 μg/g dry weight). Hence, the Zn level in SL was as high as 6 times of that in the background. The ratios of mean MFs Zn content in SL to mean background Zn content may express the availability of Zn^{2+} to the MFs synapses, suggesting the role of Zn^{2+} in the MFs to CA3 pathway. The intracellular Zn^{2+} concentration is tightly controlled by the zinc transporter 3 (ZnT3; Palmiter et al., 1996), which is found in high abundance in MFs. ZnT3 facilitates the accumulation of Zn^{2+} in MFs synaptic vesicles. Evidences have shown that Zn^{2+} is released in the same manner as neurotransmitters by excitation of MFs (Li et al., 2001; Huang et al., 2008), indicating its role for synaptic neurotransmission. Therefore, regulation on intracellular Zn^{2+} concentration in MFs is critical for the brain health and function.

Our results confirm the observation that the unbound Zn^{2+} in the brain are mostly sequestered in the mossy fiber synapses at SL and SP layers of the CA3 regions in hippocampus (Frederickson, 1989; Frederickson and Moncrieff, 1994; Frederickson et al., 2000). In addition, we have shown that nuclear microscopy is a useful approach in measuring the total Zn concentration in different layers of hippocampal CA3. Moreover, the present findings provide a precise estimate of Zn concentrations in MFs and pave the way for analysis of changes in free and bound Zn consequent to the establishment of behavioral plasticity such as memory which is an important function of the MF system.

4. Discussion and conclusion

Nuclear microscopy based approaches have previously been employed in visualizing the morphology of tissues, and analyzing the trace elemental composition and concentrations in mammalian brain. For example, the nuclear microscopic study showed an increase in calcium concentration in the rat hippocampus after kainate-induced neuronal injury (Ong et al., 1999). It was also reported that both Fe and Zn concentrations were elevated in the amyloid deposits in the brains of Alzheimer's disease transgenic mice (Rajendran et al., 2005, 2009). Recently, Barapatre et al., 2010 demonstrated the trace element mapping in Parkinsonian brain by quantitative ion beam microscopy. Hence, nuclear microscopy has become a mature and useful technique, which is capable of elemental analysis in brain samples.

It is well established that Zn works as a critical player in the CNS especially in the mossy MFs to CA3 region. In particular, synaptically released Zn has been indicated as an essential secondary messenger for the induction of LTP (long term potentiation) at the MFs to CA3 synapses of hippocampus (Li et al., 2001; Huang et al., 2008). Therefore, alterations of the intracellular Zn concentration in these areas of CNS could be one of the possible mechanisms leading to memory loss and disorders such as Alzheimer's disease. The content of Zn in the mammalian CNS has been mostly investigated using histochemistry staining methods such as Timm's stain. For example, Timm's staining on brain tissues showed the accumulation of Zn^{2+} in mossy fiber synapses of the hilar and CA3 regions (SL, SP and SO) in hippocampus (Frederickson, 1989; Frederickson and Moncrieff, 1994; Frederickson et al., 2000). However, since the focus of those previous works was to optimize the conditions for the localizations of Zn in CNS, the simultaneous trace elemental analysis of Zn was not carried out. Histochemical staining is a semi-quantitative method at best, and therefore there is an obvious need to develop a new analytical strategy that can precisely determine the Zn distribution and concentration in the brain. In order to calculate the accurate concentration of Zn in the brain, stable-isotope dilution mass spectrometry and fluorescence labeling methods were employed in the previous reports (Frederickson et al., 1983; Tomat and Lippard, 2010). Fluorescent sensors are popular tools to map the spatial and temporal distribution of Zn^{2+} using living cells. Usually, the fluorescent Zn^{2+}

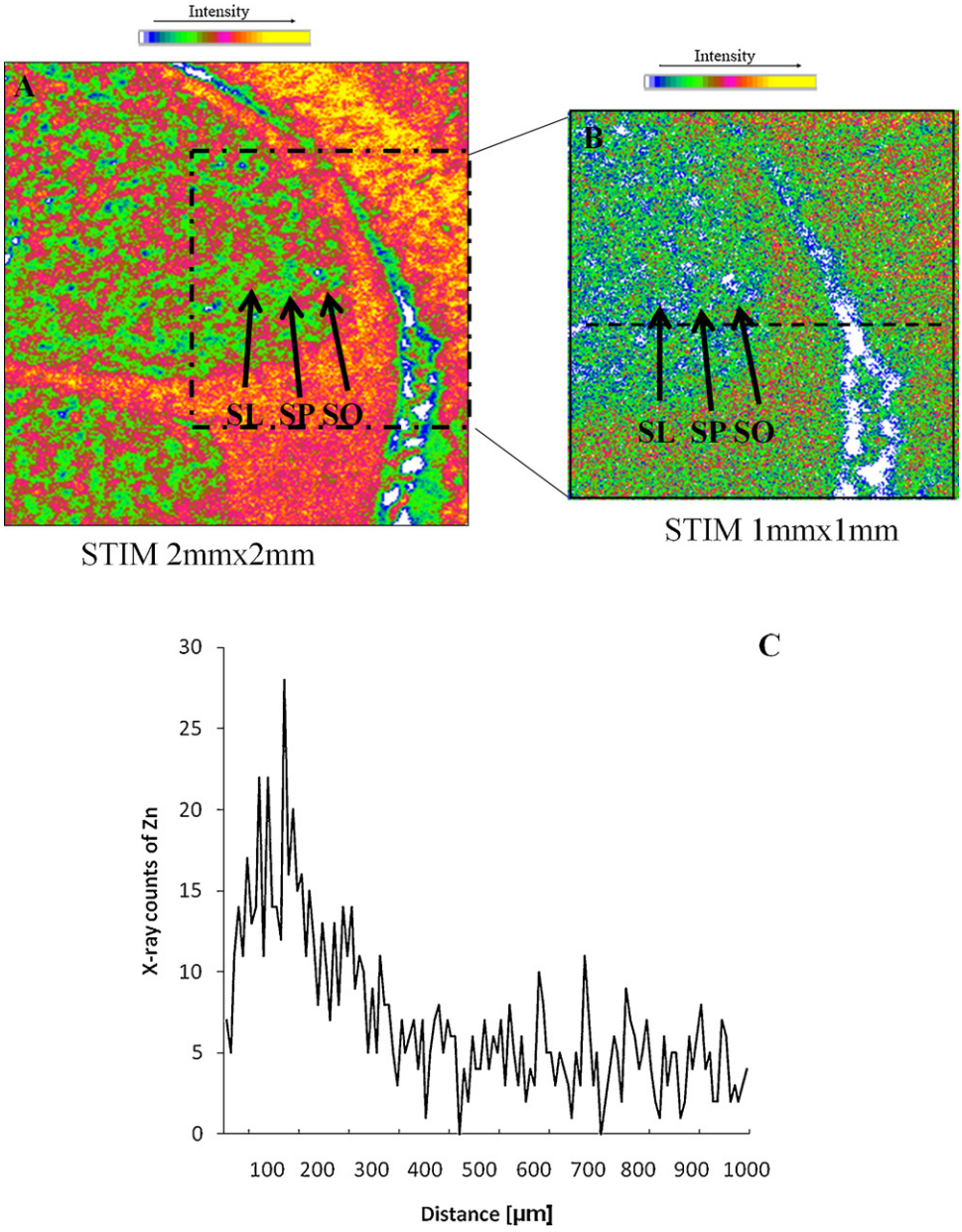

Fig. 4. Elemental zinc profile across the layers of CA3. (A) STIM mapping of the area of interest containing mossy fibers – CA3 (scan size 2 mm × 2 mm); (B) STIM mapping of the area of interest containing three layers of CA3 (scan size 1 mm × 1 mm). The dotted line represents the position of the line scan, crossing the layers of CA3. (C) Zn X-ray intensity profile. Line scan plot of the X-ray counts of Zn versus marked line scan distance. (SL: *stratum oriens*; SP: *stratum pyramidale*; SL: *stratum lucidum*). The intensity of color scale indicates changes of the area density from low to high. (For interpretation of the references to color in this figure legend, the reader is referred to the web version of the article.)

probes are microinjected into living cells and observed through fluorescent imaging. However, the efficient conditions like the stability of the labeling, sensitivity of observation as well as the isotopic exchange reactions need to be considered while using the conventional approaches. Moreover, although these fluorescent probes are capable of imaging the intracellular Zn, they cannot provide accurate information about the quantitative changes in Zn^{2+} concentrations.

So far, quantitative elemental analysis of Zn in rat hippocampus has been performed using the technique of PIXE spectroscopy by a few groups. For example, the average concentration of Zn in the rat hippocampus (Kemp and Danscher, 1979) and the maximum MFs Zn level in specific area of the hippocampal hilar were obtained (Wensink et al., 1987) in different studies. Both of the studies showed the X-ray spectrum of trace elements by PIXE, however, without Zn mapping in sub-areas of the hippocampus. In addition, Zn concentration was extracted from PIXE spectrum only at ppm (dry weight) level without molar concentration data. The information of Zn concentrations in wet tissues is less explored. As widely accepted, there has been accumulating evidences on the critical biological functions of Zn in maintaining the brain health and its performance. For example, Zn functions as neurotransmitters in the MFs terminals. Therefore, it is desirable to investigate the total Zn concentrations in the synapses of the MFs terminals to CA3 neurons in wet tissues.

To date, the present study serves as the first attempt to determine the Zn concentration in μg/g dry weight level as well as molar concentration in wet weight level in the three strata (SL, SO and SP) of hippocampal CA3 region in unstained tissue, providing data of using high resolution nuclear microscopy to identify

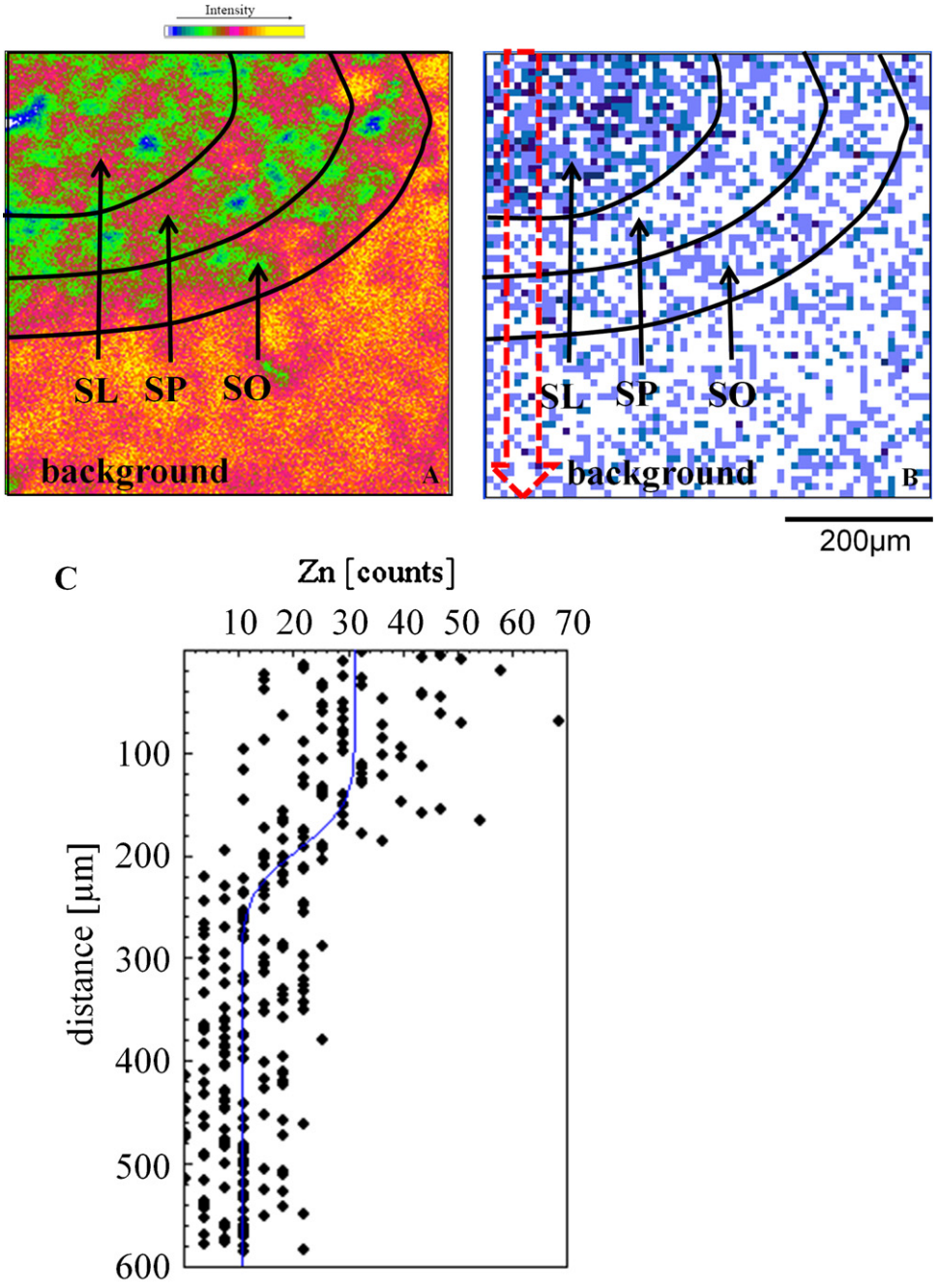

Fig. 5. (A) STIM image of the region encompassing the SL, SP and SO (scan size 600 μm × 600 μm; (B) PIXE image of the Zn distribution of the same region; (C) line scan plot of the X-ray counts of Zn carried out from SL to SO as indicated by the dotted arrow in B, shows the pronounced change in Zn level between the layers of CA3. The intensity of color scale indicates changes of the area density from low to high. (For interpretation of the references to color in this figure legend, the reader is referred to the web version of the article.)

specific features of the rat brain and to map and quantify Zn in selected areas. With the ability to focus MeV ion beams down to submicron spot sizes, and the combination of PIXE, RBS and STIM, nuclear microscopy is able to image the morphology of biomedical tissue, map trace elements like Zn and measure them down to μg/g dry weights level, without any chemical treatment of the samples. This approach may prove useful for future studies of memory in which MF growth is induced after learning (Holahan et al., 2007; Rekart et al., 2007; Routtenberg, 2010) as well as studies in which memory is dysfunctional such as Alzheimer's disease as it will allow the quantitative monitoring of variations in the Zn concentration in the CNS and its correlation with memory disease.

Acknowledgements

This work was supported in part by grants from the National University of Singapore (NUS) and SBIC RP C-013/2007 (R-144-000-227-305). While this project was carried out while Dr. Routtenberg was Distinguished Visiting Professor in the Department of Medicine, Yong Loo Lin School of Medicine, NUS.

References

Barapatre, N., Morawski, M., Butz, T., Reinert, T., 2010. Trace element mapping in Parkinsonian brain by quantitative ion beam microscopy. Nuclear Instruments and Methods B 268, 11–12.

Berg, J.M., Shi, Y., 1996. The galvanization of biology: a growing appreciation for the roles of zinc. Science 271, 1081–1085.
Besser, L., Chorin, E., Sekler, I., Silverman, W.F., Atkin, S., Russell, J.T., Hershfinkel, M., 2009. Synaptically released zinc triggers metabotropic signaling via a zinc-sensing receptor in the hippocampus. Journal of Neuroscience 29, 2890–2901.
Brewer, G.J., Aster, J.C., Knutsen, C.A., Kruckeberg, W.C., 1979. Zinc inhibition of calmodulin: a proposed molecular mechanism of zinc action on cellular functions. American Journal of Hematology 7, 53–60.
Brown, H., Peerson, J.M., Allen, L.H., Rivera, J., 2002. Effect of supplemental zinc on the growth and serum zinc concentrations of pre-pubertal children: a meta-analysis of randomized, controlled trials. American Journal of Clinical Nutrition 75, 1062–1071.
Coleman, J.E., 1998. Zinc enzymes. Current Opinion in Chemical Biology 2, 222–234.
Daiyasu, H., Osaka, K., Ishino, Y., Toh, H., 2001. Expansion of the zinc metallo-hydrolase family of the beta-lactamase fold. FEBS Letters 503, 1–6.
Danscher, G., 1981. Histochemical demonstration of heavy metals. A revised version of the sulphide silver method suitable for both light and electronmicroscopy. Histochemistry 71, 1–16.
Danscher, G., 1996. The autometallographic zinc–sulphide method. A new approach involving in vivo creation of nanometer-sized zinc sulphide crystal lattices in zinc-enriched synaptic and secretory vesicles. Histochemical Journal 28, 361–373.
Danscher, G., Howell, G., Perez-Clausell, J., Hertel, N., 1985. The dithizone, Timm's sulphide silver and selenium methods demonstrate a chelatable pool of zinc in CNS. Histochemistry 83, 419–422.
Drayer, B., Burger, P., Darwin, R., Riederer, S., Herfkens, R., Johnson, G.A., 1986. Magnetic resonance imaging of brain iron. American Journal of Roentgenology (AJR) 147, 103–110.
Frederickson, C.J., Klitenick, M.A., Manton, W.I., Kirkpatrick, J.B., 1983. Cytoarchitectonic distribution of zinc in the hippocampus of man and the rat. Brain Research 273, 335–339.
Frederickson, C.J., 1989. Neurobiology of zinc and zinc-containing neurons. International Review of Neurobiology 31, 145–238.
Frederickson, C.J., Hernandez, M.D., McGinty, J.F., 1989. Translocation of zinc may contribute to seizure-induced death of neurons. Brain Research 480, 317–321.
Frederickson, C.J., Moncrieff, D.W., 1994. Zinc-containing neurons. Biological Signals 3, 127–139.
Frederickson, C.J., Suh, S.W., Silva, D., Thompson, R.B., 2000. Importance of zinc in the central nervous system: the zinc-containing neuron. Journal of Nutrition 130, 1471.S–1483.S.
Fujii, T., 1954. Presence of zinc in nucleoli and its possible role in mitosis. Nature 174, 1108–1109.
Fujii, T., Utida, S., Mizuno, T., 1955. Reaction of starfish spermatozoa to histidine and certain other substances considered in relation to zinc. Nature 176, 1068–1069.
Grime, G.W., Dawson, M., 1994. A PC-based data acquisition package for nuclear microbeam systems. Nuclear Instruments and Methods B 89, 223–228.
Ho, E., Ames, B.N., 2002. Low intracellular zinc induces oxidative DNA damage, disrupts p53, NFkappa B, and AP1 DNA binding, and affects DNA repair in a rat glioma cell line. Proceedings of the National Academy of Sciences of the United States of America 99, 16770–16775.
Holahan, M.R., Honegger, K.S., Routtenberg, A., 2007. Expansion and retraction of hippocampal mossy fibers during post-weaning development: strain-specific effects of NMDA receptor blockade. Hippocampus 17, 58–67.
Huang, Y.Z., Pan, E., Xiong, Z.Q., McNamara, J.O., 2008. Zinc-mediated transactivation of TrkB potentiates the hippocampal mossy fiber-CA3 pyramid synapse. Neuron 57, 546–558.
Hubbard, S.R., Bishop, W.R., Kirschmeier, P., George, S.J., Cramer, S.P., Hendrickson, W.A., 1991. Identification and characterization of zinc binding sites in protein kinase C. Science 254, 1776–1779.
Jackson, B., Harper, S., Smith, L., Flinn, J., 2006. Elemental mapping and quantitative analysis of Cu, Zn, and Fe in rat brain sections by laser ablation ICP-MS. Analytical and Bioanalytical Chemistry 384, 951–957.
Johansson, S.A.E., Campbell, J.L., Malmqvist, K.G., 1995. Particle Induced X-Ray Emission Spectrometry (PIXE). John Wiley & Sons, Chichester, U.K.
Kemp, K., Danscher, G., 1979. Multi-element analysis of the rat hippocampus by proton induced X-ray emission spectroscopy (phosphorus, sulphur, chlorine, potassium, calcium, iron, zinc, copper, lead, bromine, and rubidium). Histochemistry 59, 167–176.
Lengyel, I., Fieuw-Makaroff, S., Hall, A.L., Sim, A.T., Rostas, J.A., Dunkley, P.R., 2000. Modulation of the phosphorylation and activity of calcium/calmodulin-dependent protein kinase II by zinc. Journal of Neurochemistry 75, 594–605.
Li, Y., Hough, C.J., Frederickson, C.J., Sarvey, J.M., 2001. Induction of mossy fiber3-CA3 long-term potentiation requires translocation of synaptically released Zn^{2+}. Journal of Neuroscience 21, 8015–8025.
Lippard, S.J., Berg, J.M., 1994. Principles of Bioinorganic Chemistry. University Science Books, Mill Valley, CA.
Lutsenko, S., Bhattacharjee, A., Hubbard, A.L., 2010. Copper handling machinery of the brain. Metallomics 2, 596–608.
MacDonald, R.S., 2000. The role of zinc in growth and cell proliferation. Journal of Nutrition 130, 1500S–1508S.
Maret, W., Jacob, C., Vallee, B.L., Fischer, E.H., 1999. Inhibitory sites in enzymes: zinc removal and reactivation by thionein. Proceedings of the National Academy of Sciences of the United States of America 96, 1936–1940.
O'Halloran, T.V., 1993. Transition metals in control of gene expression. Science 261, 715–724.
Ong, W.Y., Ren, M.Q., Makjanic, J., Lim, T.M., Watt, F., 1999. A nuclear microscopic study of elemental changes in the rat hippocampus after kainate-induced neuronal injury. Journal of Neurochemistry 72, 1574–1579.
Palmiter, R.D., Cole, T.B., Quaife, C.J., Findley, S.D., 1996. ZnT-3, a putative transporter of zinc into synaptic vesicles. Proceedings of the National Academy of Sciences 93, 14934–14939.
Paoletti, P., Vergnano, A.M., Barbour, B., Casado, M., 2009. Zinc at glutamatergic synapses. Neuroscience 158, 126–136.
Park, J.A., Koh, J.Y., 1999. Induction of an immediate early gene egr-1 by zinc through extracellular signal-regulated kinase activation in cortical culture: its role in zinc-induced neuronal death. Journal of Neurochemistry 73, 450–456.
Paxinos, G., Watson, C., 2007. The Rat Brain in Stereotaxic Coordinates, 6th ed. Elsevier, San Diego, USA.
Prasad, A.S., Halsted, J.A., Nadimi, M., 1961. Syndrome of iron deficiency anemia, hepatosplenomegaly, hypogonadism, dwarfism and geophagia. American Journal of Medicine 31, 532–546.
Prasad, A.S., 1996. Zinc: The biology and therapeutics of an ion. Annals of Internal Medicine 125, 142–144.
Quest, A.F., Bloomenthal, J., Bardes, E.S., Bell, R.M., 1992. The regulatory domain of protein kinase C coordinates four atoms of zinc. Journal of Biological Chemistry 267, 10193–10197.
Rajendran, R., Ren, M.Q., Casadesus, G., Smith, M.A., Perry, G., Huang, E., Ong, W.Y., Halliwell, B., Watt, F., 2005. Nuclear microscopy of diffuse plaques in the brains of transgenic mice. Nuclear Instruments and Methods B 231, 326–332.
Rajendran, R., Ronald, J.A., Ye, T., Ren, M.Q., Chen, J.W., Weissleder, R., Rutt, B.K., Halliwell, B., Watt, F., 2009. Nuclear microscopy: a novel technique for quantitative imaging of gadolinium distribution within tissue sections. Microscopy and Microanalysis 15, 338–344.
Rekart, J.L., Sandoval, J., Bermudez-Rattoni, F., Routtenberg, A., 2007. Remodeling of hippocampal mossy fibers is selectively induced seven days after the acquisition of a spatial but not a cued memory task. Learning and Memory 14, 416–421.
Ren, M.Q., Watt, F., Huat, B.T., Halliwell, B., 2003. Correlation of iron and zinc levels with lesion depth in newly formed atherosclerotic lesions. Free Radical Biology and Medicine 34, 746–752.
Ren, M.Q., Rajendran, R., Ning, P., Tan, B.K.H., Choon, N.O., Watt, F., Jenner, A., Halliwell, B., 2006. Zinc supplementation decreases the development of atherosclerosis in rabbits. Free Radical Biology and Medicine 41, 222–225.
Routtenberg, A., 2010. Adult learning and remodeling of hippocampal mossy fibers: unheralded participant in circuitry for long-lasting spatial memory. Hippocampus 20, 44–45.
Schenck, J.F., 2003. Magnetic resonance imaging of brain iron. Journal of the Neurological Sciences 207, 99–102.
Tomat, E., Lippard, S.J., 2010. Imaging mobile zinc in biology. Current Opinion in Chemical Biology 14, 225–230.
Truong-Tran, A.Q., Carter, J., Ruffin, R.E., Zalewski, P.D., 2001. The role of zinc in caspase activation and apoptotic cell death. BioMetals 14, 315–330.
Tupler, R., Perini, G., Green, M.R., 2001. Expressing the human genome. Nature 409, 832–833.
Vallee, B.L., Falchuk, K.H., 1993. The biochemical basis of zinc physiology. Physiological Reviews 73, 79–118.
Vallee, B.L., Auld, D.S., 1993a. Cocatalytic zinc motifs in enzyme catalysis. Proceedings of the National Academy of Sciences of the United States of America 90, 2715–2718.
Vallee, B.L., Auld, D.S., 1993b. New perspective on zinc biochemistry: cocatalytic sites in multi-zinc enzymes. Biochemistry 32, 6493–6500.
Watt, F., Orlic, I., Loh, K.K., Sow, C.H., Thong, P., Liew, S.C., Osipowicz, T., Choo, T.F., Tang, S.M., 1994. The National University of Singapore nuclear microscope facility. Nuclear Instruments and Methods B 85, 708–715.
Watt, F., 1995. Nuclear microscopy in the life sciences. Nuclear Instruments and Methods B 104, 276–284.
Watt, F., Rajendran, R., Ren, M.Q., Tan, B.K.H., Halliwell, B., 2006. A nuclear microscopy study of trace elements Ca, Fe, Zn and Cu in atherosclerosis. Nuclear Instruments and Methods B 249, 646–652.
Weinberger, R.P., Rostas, J.A., 1991. Effect of zinc on calmodulinstimulated protein kinase II and protein phosphorylation in rat cerebral cortex. Journal of Neurochemistry 57, 605–614.
Wensink, J., Lenglet, W.J., Vis, R.D., Van den Hamer, C.J., 1987. The effect of dietary zinc deficiency on the mossy fiber zinc content of the rat hippocampus. A microbeam PIXE study. Histochemistry 87, 65–69.
Wood, R.J., 2000. Assessment of marginal zinc status in humans. Journal of Nutrition 130, 1350S–1354S.